Ann. Geophys., 29, 2061–2079, 2011
www.ann-geophys.net/29/2061/2011/
doi:10.5194/angeo-29-2061-2011

Annales Geophysicae

A comparison study between observations and simulation results of Barghouthi model for O^+ and H^+ outflows in the polar wind

I. A. Barghouthi[1], **S. H. Ghithan**[1], **and H. Nilsson**[2]

[1]Department of Physics, Al-Quds University, Jerusalem, Palestine
[2]Swedish Institute of Space Physics, Kiruna, Sweden

Received: 8 March 2011 – Revised: 30 September 2011 – Accepted: 12 October 2011 – Published: 22 November 2011

Abstract. To advance our understanding of the effect of wave-particle interactions on ion outflows in the polar wind region and the resulting ion heating and escape from low altitudes to higher altitudes, we carried out a comparison between polar wind simulations obtained using Barghouthi model with corresponding observations obtained from different satellites. The Barghouthi model describes O^+ and H^+ outflows in the polar wind region in the range 1.7 R_E to 13.7 R_E, including the effects of gravity, polarization electrostatic field, diverging geomagnetic field lines, and wave-particle interactions. Wave-particle interactions were included into the model by using a particle diffusion equation, which depends on diffusion coefficients determined from estimates of the typical electric field spectral density at relevant altitudes and frequencies. We provide a formula for the velocity diffusion coefficient that depends on altitude and velocity, in which the velocity part depends on the perpendicular wavelength of the electromagnetic turbulence $\lambda_\perp$. Because of the shortage of information about $\lambda_\perp$, it was included into the model as a parameter. We produce different simulations (i.e. ion velocity distributions, ions density, ion drift velocity, ion parallel and perpendicular temperatures) for O^+ and H^+ ions, and for different $\lambda_\perp$. We discuss the simulations in terms of wave-particle interactions, perpendicular adiabatic cooling, parallel adiabatic cooling, mirror force, and ion potential energy. The main findings of the simulations are as follows: (1) O^+ ions are highly energized at all altitudes in the simulation tube due to wave-particle interactions that heat the ions in the perpendicular direction, and part of this gained energy transfer to the parallel direction by mirror force, resulting in accelerating O^+ ions along geomagnetic field lines from lower altitudes to higher altitudes. (2) The effect of wave-particle interactions is negligible for H^+ ions at altitudes below $\sim$7 R_E, while it is important for altitudes above 7 R_E. For O^+ wave particle interaction is very significant at all altitudes. (3) For certain $\lambda_\perp$ and at points, altitudes, where the ion gyroradius is equal to or less than $\lambda_\perp$, the effect of wave-particle interactions is independent of the velocity and it depends only on the altitude part of the velocity diffusion coefficient; however, the effect of wave-particle interactions reduce above that point, called saturation point, and the heating process turns to be self-limiting heating. (4) The most interesting result is the appearance of O^+ conics and toroids at low altitudes and continue to appear at high altitudes; however, they appear at very high altitudes for H^+ ions. We compare quantitatively and qualitatively between the simulation results and the corresponding observations. As a result of many comparisons, we find that the best agreement occurs when $\lambda_\perp$ equals to 8 km. The quantitative comparisons show that many characteristics of the observations are very close to the simulation results, and the qualitative comparisons between the simulation results for ion outflows and the observations produce very similar behaviors. To our knowledge, most of the comparisons between observations (ion velocity distribution, density, drift velocity, parallel and perpendicular temperatures, anisotropy, etc.) and simulations obtained from different models produce few agreements and fail to explain many observations (see Yau et al., 2007; Lemaire et al., 2007; Tam et al., 2007; Su et al., 1998; Engwall et al., 2009). This paper presents many close agreements between observations and simulations obtained by Barghouthi model, for O^+ and H^+ ions at different altitudes i.e. from 1.7 R_E to 13.7 R_E.

Keywords. Space plasma physics (Wave-particle interactions)

Correspondence to: I. A. Barghouthi
(barghouthi@science.alquds.edu)

Published by Copernicus Publications on behalf of the European Geosciences Union.

1 Introduction

A variety of plasma flows along open magnetic field lines can be found in the solar-terrestrial plasma systems, for example, solar wind (a supersonic expansion of plasma blowing out of the solar corona) and polar wind (an ambipolar outflow of thermal plasma from the terrestrial ionosphere at high latitudes to the magnetosphere along open geomagnetic field lines of the Earth). The purpose of this paper is to review the observations related to O^+ and H^+ ions outflows in the polar wind in order to compare them with the corresponding simulations obtained by using Barghouthi model (Barghouthi, 2008). We expect from this comparison to shed light on the significant role of wave-particle interaction in controlling the ion outflow in the polar wind region. We also want to discuss the potential role of finite wavelength effects (i.e. velocity dependent velocity diffusion coefficients), and provide the scientific community with the wavelength of the electromagnetic turbulence that best matches many of the observed features. The Barghouthi model can provide a good match to many observations, and we expect that we have a lot to learn also from the cases with poor agreement, which we also discuss.

In particular we want to improve our understanding of the role of wave-particle interactions in the polar wind region, and highlight the role of finite wavelength effects and how these affect the observed ion velocity distributions and the altitude distributions of the ion moments. We limit our study to the polar cap, i.e. the polar wind region. This is in contrast to the outflow in the auroral region, and in particular from the cusp, where wave activity is higher and the velocity diffusion coefficients are higher.

Many observations related to the ion outflows in the polar cap region have motivated different theoretical studies to provide the mechanism (mechanisms) that is (are) responsible for these observations. Hoffman and Dobson (1980) summarized polar wind data obtained by Explorer 33 and ISIS-2 under different geophysical conditions. The characteristics of the polar wind mentioned in that paper and other polar wind measurements obtained by several space instruments aboard DE-1 satellite were the major source of observations for comparisons with different polar wind models. Lemaire et al. (2007) reviewed the history of kinetic polar wind models and early observations (i.e. observations of the polar wind conducted by space instruments before the data from Akebono and Polar satellites were available). They found that theoretical models constructed to explain these observations did not explain the nature of cool O^+ ions observed in the polar wind.

Another generation of observations provided more important results: (1) The observations of supersonic outflows of H^+ ions by DE-1 satellite have been confirmed by Nagai et al. (1984), i.e. the supersonic nature of polar wind. (2) Gurgiolo and Burch (1982) and Waite et al. (1985) investigated the measurements of DE-1 and observed the suprathermal O^+ ions with supersonic speed in the polar cap region. (3) Abe et al. (1993) used the measurements conducted by Akebono satellite and found that O^+ ion outflows turned to be supersonic outflow at altitudes around 11 000 km and they confirmed that the source of O^+ ions in the polar wind is from the polar ionosphere. In addition, they found that O^+ ions outflow velocity monotonically increased with altitude, attaining supersonic flow at 10 000 km, and O^+ ions observed to be the dominant ions at high altitudes. (4) Gurgiolo and Burch (1982) confirmed the existence of O^+ ions at altitude 20 000 km by analyzing data obtained by High Altitude Plasma Instrument (HAPI) aboard DE-1 satellite; they found that O^+ ions temperature is 2.75 eV due to perpendicular heating in regions located at lower altitudes in the polar wind. (5) Green and Waite (1985) reported a number of events of outflowing O^+ ions observed by the Retarding Ion Mass Spectrometer (RIMS) aboard DE-1 satellite.

As an example of more recent reports, Chugunin (2009) studied the polar wind by analyzing the measurements obtained by the Hyperboloid mass-spectrometer installed onboard the Interball Auroral probe satellite at heights of $\sim$20 000 km. After the analysis of the moments of the velocity distribution function – namely, the densities, field-aligned velocities, and temperatures of the ions in the polar wind region – a comparison between the characteristics of thermal ion outflows in the polar cap region with the results of theoretical models has been conducted. The comparison showed that the current models of the polar wind did not describe well these observations; he found that the temperatures are substantially higher than the model ones, and the measured field-aligned velocities of O^+ fluxes are several times higher than the model ones.

Recently it has become possible to measure low energy ion fluxes in the magnetotail lobes by analyzing the wake electric field created by cold plasma streaming past a positively charged spacecraft (Engwall et al., 2009). Nilsson et al. (2010) studied the centrifugal acceleration of the ions in this magnetotail lobe data set and found it to be rather small, much less than in the high altitude (above 5 R_E) cusp related ion outflow reported in Nilsson et al. (2006, 2008). Demars et al. (1996) also studied the effect of centrifugal acceleration with a particle in cell code and found that it was not significant at low altitude. Polar wind and cusp-related outflow will mix above the polar cap and in the magnetotail lobes, depending on the starting point and parallel velocities of the outflowing ions. The magnetotail lobe ions are the ones starting well into the polar cap (away from the cusp) and/or with a long transport time (low velocity for a significant part of its transport path). It thus depends on the transport path of the ions if we expect centrifugal acceleration to be important or not. In this paper we do not include centrifugal acceleration, but will discuss how much this neglecting affects our results. Away from the cusp, a model of the polar wind region, which we use here, is suitable regardless of the starting point of the ions, but the changing initial conditions between

different regions may give discrepancies between our model results (which use fixed initial conditions) and observations.

Regarding the observations of the ion velocity distribution functions, non-Maxwellian ion velocity distributions such as elevated conics and toroids have been reported in the different high-latitudes regions (Winningham and Burch, 1984; Huddleston et al., 2000; Waara et al., 2010; Slapak et al., 2011). Particle measurements performed onboard the Dynamics Explorer 1 (DE-1) satellite have revealed the existence of a population of O^+ ion conic extended in latitude throughout the equatorward portion of the auroral zone (Winningham and Burch, 1984). Huddleston et al. (2000) examined events where the TIDE and TIMAS ion instruments onboard the Polar spacecraft observed transversely accelerated ions at high altitudes equatorward of the cusp. They reported both H^+ and O^+ populations' heated perpendicular to the local geomagnetic field and the heated ions (H^+ and O^+) had the form of toroids in velocity space.

Because of the observational features of the polar wind, two terms appeared in the literature: they are classical polar wind and non-classical polar wind. The classical polar wind theory related to O^+ and H^+ ion outflows assumed that transport and dynamic effects control the behavior of these ions. However, in the non-classical polar wind theory, the effects of wave-particle interaction, centrifugal acceleration, and other mechanisms affect ion outflows in the polar wind (Tam et al., 2007). Most of the models of the classical polar wind theory did not deal with O^+ ions but they dealt with H^+ outflows. As mentioned above, Lemaire et al. (2007) reviewed early observations of polar wind and Yau et al. (2007) continued and reviewed recent observations of polar wind. They concluded that satellite-borne ion composition observations over the past 4 decades have confirmed the existence of the polar wind as well as its basic characteristics. These observations cover the altitude range from 1000 km to 50 500 km above the polar cap region and revealed several features of the polar wind that are unexpected from the classical polar wind theories. Some of these features are the day-night asymmetry in polar wind velocity, appreciable O^+ outflow at high altitudes, and significant electron temperature anisotropy in the sunlit polar wind. In addition, Yau et al. (2007) raised several questions related to the polar wind still unresolved, such as the relative contribution of the different sources of the high-altitude O^+ polar wind, and the relative importance between the classical and non-classical ion acceleration mechanisms. In particular they noted as an outstanding question that it is possible that the cusp (i.e. cleft ion fountain) could be the sole source for O^+ ions in the polar cap.

In this paper, we tabulate different observations for O^+ and H^+ ion outflows in the polar wind that covers the altitude range from 1.7 R_E to 13.7 R_E obtained from different satellites, in order to compare it with the corresponding simulation results from Barghouthi model. This paper is organized as follows: theoretical formulations are presented in Sect. 2. We present polar wind simulations in Sect. 3. In Sect. 4, we compare between the simulation results for both O^+ and H^+ ions and the corresponding observations. In Sect. 5, we present the conclusions.

2 Theoretical formulations

The continuous outflow of thermal plasma escaping from the polar ionosphere at high latitudes to the magnetosphere along "open" geomagnetic field lines is called the polar wind (Axford, 1968). The outflow consists of light thermal H^+ ions and heavy energized O^+ ions and electrons. There are many external forces and processes that affect this polar wind outflow, such as gravitational force, polarization electrostatic field, mirror force, collisions between ions, and the interaction between ions and the electromagnetic turbulences (i.e. wave-particle interactions). It is convenient to describe each ion species in the polar wind plasma by a separate velocity distribution function $f_s(v_s, r_s, t)$. This velocity distribution function is changed with time due to the effects of these external forces, collisions of ions, and wave-particle interactions. The mathematical description of this evolution process in time is given by the well-known Boltzmann equation:

$$\frac{\partial f_s}{\partial t} + v_s \cdot \nabla f_s + \left[\boldsymbol{g} + \frac{e_s}{m_s} \left(\boldsymbol{E} + \frac{1}{c} v_s \times \boldsymbol{B} \right) \right] \cdot \nabla_{vs} f_s = \frac{\delta f_s}{\delta t} \quad (1)$$

where ($\boldsymbol{g}$) is the acceleration of gravity, ($\boldsymbol{E}$) is the polarization electrostatic field, ($\boldsymbol{B}$) is the geomagnetic field, (e_s, m_s) are the charge and the mass of the ion (i.e. either H^+ or O^+, respectively), (c) is the speed of light, ($\partial/\partial t$) is the time derivatives, (∇) is the coordinate space gradient, and (∇_{vs}) is the velocity space gradient. The right-hand side of the Boltzmann equation ($\delta f_s/\delta t$) represents the rate of change of $f_s(v_s, r_s, t)$ in a given region of phase space, (v_s, r_s) as a result of collisions and wave-particle interactions.

In this study, we are interested in the collisionless region of the polar wind, i.e. the ions move in the simulation tube which extends from 1.7 R_E to 13.7 R_E under the effects of gravitational force, polarization electrostatic field, diverging geomagnetic field, and wave-particle interactions. The potential energy profile $\phi(r)$ owing to gravitational force and polarization electrostatic field is given by

$$\phi(r) = kT_e \ln\left(\frac{n_e}{(n_e)_o}\right) + (GM_E m)\left(\frac{1}{1.7\,R_E} - \frac{1}{r}\right) \quad (2)$$

where (k) is Boltzmann's constant; (T_e) is the electron temperature; (n_e) and ($n_e)_0$ are the electron densities at r and 1.7 R_E, respectively, which can be calculated from the quasi-neutrality condition ($n_e = n(O^+) + n(H^+)$); (G) is the gravitational constant; M_E is the mass of the Earth; and m is the ions mass. The geomagnetic field $\boldsymbol{B}$ was taken to be proportional to r^{-3} where r is the geocentric distance. At very high altitudes, the real $\boldsymbol{B}$ field may fall off at a slower rate,

which would yield higher perpendicular temperatures and lower parallel velocities than what we obtain in our model.

As mentioned above, there are many observations (Abe et al., 1993; Su et al., 1998; Yau et al., 2007; Huddleston et al., 2000; etc.) at high-altitudes and high-latitudes such as ions density, drift velocity, temperature, non-Maxwellian features of H^+ and O^+ ion velocity distributions, and the existence of heavy and energized O^+ ions, obtained from several polar orbiting satellites. These observations of the ion outflows in the polar wind and auroral regions need to be explained theoretically in order to understand which mechanisms are responsible for producing these features and behaviors of the polar wind ions.

Many theoretical studies (Chang and Coppi, 1981; Chang et al., 1986; Retterer et al., 1987a, b, 1994; Crew et al., 1990; Barghouthi, 1997, 2008; Barghouthi and Atout, 2006; Bouhram et al., 2003a, b, 2004, and others) concluded that it is very essential to take into consideration the effect of wave-particle interactions when investigating auroral and cusp ion outflows. Also, Barakat and Barghouthi (1994); Barghouthi et al. (1998); Lemaire et al. (2007); and Tam et al. (2007) found that wave-particle interactions (WPI) play an important role in determining the behavior of ion outflows in the polar wind region. To include the effect of WPI in a collisionless region, we replace the right-hand side of Boltzmann equation by the term that represents the interaction between ions and the electromagnetic turbulence, which is resonant interactions at ion gyrofrequency. This is represented by particle diffusion equation in the velocity space and is given by Retterer et al. (1987a):

$$\left[\frac{\delta f_j}{\delta t}\right]_{\mathrm{WPI}} = \left(\frac{1}{v_\perp}\right)\frac{\partial}{\partial v_\perp}\left[D_{\perp j} v_\perp \frac{\partial f_j}{\partial v_\perp}\right] \tag{3}$$

where $(D_\perp)$ is the quasi-linear velocity diffusion coefficient. The influence of WPI on the ion during (Δt) is taken into consideration by incrementing the ion's perpendicular velocity by a random increment $(\Delta v_\perp)$, such as the ion heating rate due to these random increments is consistent with the velocity diffusion coefficient:

$$\left\langle (\Delta v_\perp)^2 \right\rangle = 4 D_\perp \Delta t \tag{4}$$

where (Δt) is the time interval chosen randomly and $(D_\perp = (1/2\,\mathrm{m})\ dW_{\mathrm{wave}}/dt)$ is the velocity diffusion coefficient, (dW_{wave}/dt) is the ion heating rate due to wave particle interaction and (m) is the ion mass. It is important to note that the two components of $\Delta v_\perp$ in the plane perpendicular to the geomagnetic field lines are chosen to be Gaussian random variables such as $\left\langle \Delta v_x^2 \right\rangle = \left\langle \Delta v_y^2 \right\rangle = 2 D_\perp \Delta t$; the vector $\Delta v_\perp$ is added to the ion's transverse velocity, assuming a random orientation with respect to the gyrophase.

The time step Δt should be infinitesimal $(\Delta t \to 0)$. However, as Δt decreases, the computational time increases. In order to select an optimum value of Δt that strikes a compromise between speed and accuracy, the simulation was repeated for successively decreasing value of Δt until the results became insensitive to the specific value of Δt. In particular, the optimum value of the time step was found to be $\Delta t \sim 0.01 v_{\mathrm{th}}^2 \big/ D_\perp$, where v_{th} is the thermal speed of the ion species that is being simulated. This condition guarantees that the average velocity perturbation per unit time step is much smaller than the thermal speed of the ambient ions. We notice that Δt depends on both the ion's type and its position.

Barghouthi (1997) and Barghouthi et al. (1998) computed the altitude dependence of $(D_\perp)$ by analyzing experimental data of electric field spectral density obtained by PWI onboard the DE-1 satellite (i.e. for high solar activity conditions); they obtained the following expression for the velocity diffusion coefficient $D_\perp$ in the polar wind region:

$$D_\perp(r) = \left\{ \begin{array}{l} 5.77\times 10^3 (r \big/ R_{\mathrm{E}})^{7.95}\ \mathrm{cm^2\,s^{-3}}, \quad \text{for } H^+ \\ 9.55\times 10^2 (r \big/ R_{\mathrm{E}})^{13.3}\ \mathrm{cm^2\,s^{-3}}, \text{ for } O^+ \end{array} \right\} \tag{5}$$

Barghouthi (2008) developed a new form for the diffusion coefficient and found it to be velocity dependent in addition to its dependence on altitude. Finally, to model the heating process (i.e. wave-particle interactions), we specify a model for the diffusion coefficient $(D_\perp)$ as a function of perpendicular velocity $(v_\perp)$ and position (r/R_{E}) along geomagnetic field lines of the Earth. For the spatial variation (i.e. the altitude dependence), we choose the form obtained by Barghouthi et al. (1998), while for the velocity dependence, we choose the form obtained by Barghouthi (2008). The final form for $D_\perp$ is altitude and velocity dependent and given by the following expression:

$$D_\perp(r, v_\perp) = D_\perp(r) \left\{ \begin{array}{l} 1 \text{ for } \left(\frac{k_\perp v_\perp}{\Omega_{\mathrm{i}}}\right) < 1 \\ \\ \left(\frac{k_\perp v_\perp}{\Omega_{\mathrm{i}}}\right)^{-3} \text{ for } \left(\frac{k_\perp v_\perp}{\Omega_{\mathrm{i}}}\right) \geq 1 \end{array} \right\} \tag{6}$$

where the diffusion coefficient $D_\perp(r)$ is given in Eq. (5), Ω_{i} is the ion gyrofrequency, and $k_\perp$ is perpendicular wave vector and it is related to the characteristic perpendicular wavelength of the electromagnetic turbulence $\lambda_\perp$.

Introducing a velocity dependence of the velocity diffusion coefficient formally makes it more difficult to solve Eq. (3). This problem has been addressed by Retterer et al. (1983), who showed that in order to recover the quasi-linear diffusion formulation of wave-particle interactions when the diffusion coefficient has a velocity dependence, one must include two terms: a mean velocity change that is proportional to the velocity divergence of the diffusion coefficient times Δt, and a second order mean velocity change that is proportional to the diffusion coefficient times Δt (i.e. Eq. 4). If the velocity dependence of the diffusion coefficient is weak, as it is for ion cyclotron wave interactions, then the term related to the mean velocity change can be ignored (J. Retterer, personal communications, 2010).

Now, all cards in Boltzmann equation are on the table. To solve this equation, i.e. to find the velocity distribution function $f_{\mathrm{s}}(v_{\mathrm{s}}, r_{\mathrm{s}}, t)$ and its velocity moments, we will

use Barghouthi model that has been explained and tested in Barghouthi (2008). In that model, the ion is injected into the simulation region at the lower boundary (i.e. 1.7 R_E) with a random initial velocity that corresponds to the ion velocity distribution immediately below the lower boundary; the ion moves under the influence of gravitational force, polarization electrostatic field (the altitude profile for the potential energy due to these forces is presented in Fig. 1), mirror force, and the effect of WPI. In the simulation tube and at different altitudes, statistical data were accumulated about the injected ions and finally it has been used to compute the velocity distribution function and the following velocity moments:

$$n_s = \int f_s(v_s) d^3 v_s \tag{7}$$

$$u_s = \frac{\int v_{lls} f_s(v_s) d^3 v_s}{\int f_s(v_s) d^3 v_s} \tag{8}$$

$$T_{lls} = \frac{\frac{m_s}{k} \int (v_{lls} - u_s)^2 f_s(v_s) d^3 v_s}{\int f_s(v_s) d^3 v_s} \tag{9}$$

$$T_{\perp s} = \frac{\frac{m_s}{2k} \int v_\perp^2 f_s(v_s) d^3 v_s}{\int f_s(v_s) d^3 v_s} \tag{10}$$

In the above equations, "s" denotes the type of the ion (i.e. H^+ or O^+); Eqs. (7)–(10) are the ion density, drift velocity, parallel temperature, perpendicular temperature, respectively. It is important to note that here we are using the Barghouthi model with initial conditions and velocity diffusion coefficients suitable for the polar wind region. The model can also describe the auroral region; the only difference is the boundary conditions that reperesent the region and the altitude dependence (i.e. $D_\perp(r)$) of the diffusion coefficient.

3 Polar wind simulations

The boundary conditions selected for the polar wind region are similar to those of Barghouthi et al. (1998): at lower boundary (i.e. 1.7 R_E), we set the O^+ ion drift velocity at 0.0 km s^{-1}, the oxygen ion density at 100 cm^{-3}, and the O^+ ion temperature at 3000 °K. However, for H^+ ions, we set the H^+ ion drift velocity at 11 km s^{-1}, the hydrogen ion density at 200 cm^{-3}, and the H^+ ion temperature at 3000 °K. The values chosen are consistent with observations reported for this altitude range, e.g. Chandler et al. (1991), Su et al. (1998). One may note that the Su et al. (1998) study shows on average a small downward velocity for O^+ in this altitude range, but a perpendicular temperature that will lead to mirroring slightly below the observation altitude. Under such circumstances a close to zero initial velocity is a reasonable boundary condition, where the precise value should be tuned to give a reasonable number flux. The close to zero velocity of O^+ results from an approximate balance between gravity and upward forces, and can lead to long horizontal transport times. This is consistent with the cusp as the initial source of the O^+ ions. If that is the case we would expect our model to reach too low number fluxes of outflowing O^+ ions in steady state, as most outflow observed at high altitude will be caused by a gradual depletion of the drifting flux tube, i.e. steady state does not apply. The electron temperature was kept constant at 1000 °K along the entire simulation tube (1.7–13.7 R_E), this assumption is justified by the fact that it is resonable at low altitudes and the effect is negligible at high altitudes. The velocity distribution functions for both H^+ and O^+ ions are assumed to be Maxwellian at the lower boundary. Also, we considered a wide range of characteristic wavelengths for the electromagnetic turbulence ($\lambda_\perp = \infty$, 50, 20, 8, and 1 km), since the data obtained by PWI instrument aboard DE-1 spacecraft or any other satellites do not include information about the perpendicular wavelength of the electromagnetic turbulence.

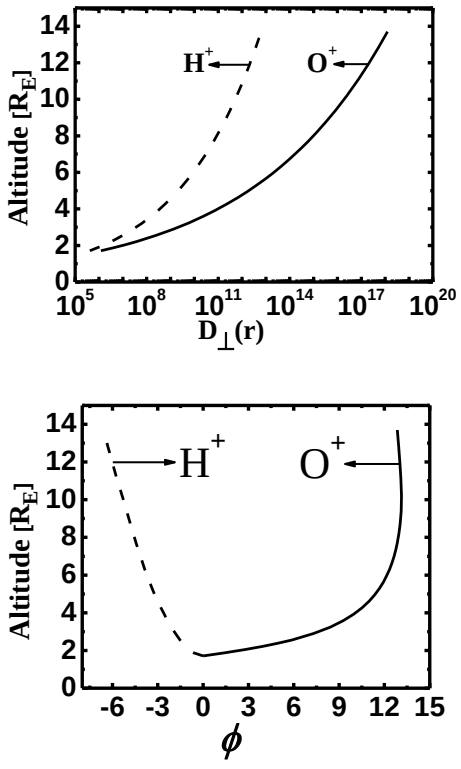

Fig. 1. Altitude profiles of ions potential energy (ϕ) due to the gravitational force and polarization electrostatic field, for O^+ ions (solid line) and H^+ ions (dashed line), when perpendicular wavelength of the electromagnetic turbulence $\lambda_\perp = 8$ km.

One question which remain regarding the boundary conditions is how dependent these are on the geomagnetic activity (Kp index), solar EUV (F10.7 cm index), season, solar zenith angle and other conditions. Any such dependence is not well established, though the dependence seems not to be very strong for the polar cap (Abe et al., 1993, 1996, 2004).

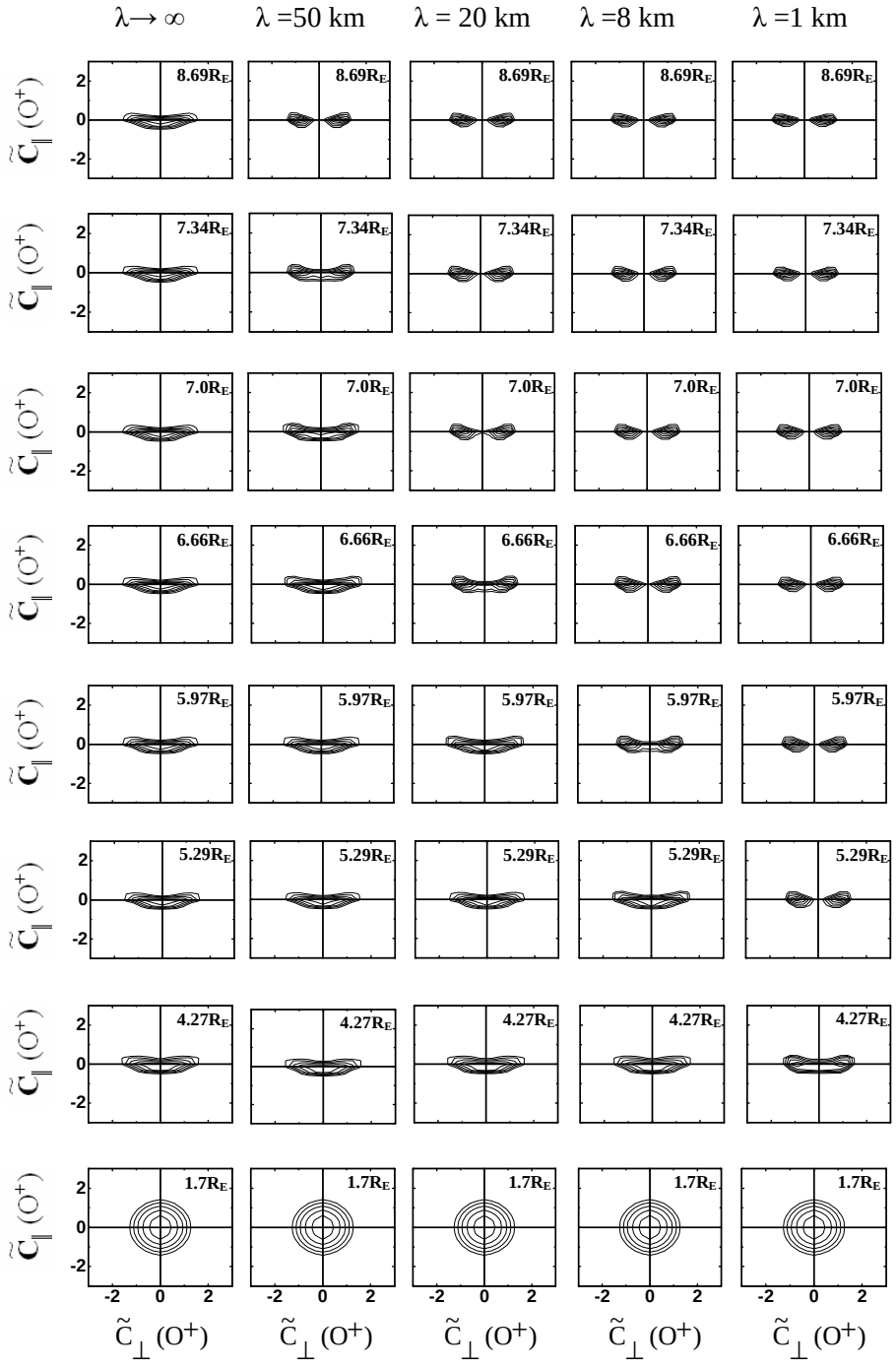

Fig. 2. O^+ ions velocity distribution functions at different geocentric distances (1.7, 4.27, 5.29, 5.97, 6.66, 7.0, 7.34 and 8.69 R_E) for different electromagnetic turbulence wavelengths ($\lambda_\perp$), the wavelengths considered here are $\lambda_\perp \to \infty$ (1st panel), $\lambda_\perp = 50$ km (2nd panel), $\lambda_\perp = 20$ km (3rd panel), $\lambda_\perp = 8$ km (4th panel), and $\lambda_\perp = 1$ km (5th panel). $f(O^+)$ is represented by equal values contours in the normalized velocity $(\tilde{c}_{||}, \tilde{c}_\perp)$ plane, where $\tilde{c} = \left[v - u(O^+)\right] / \left[2kT(O^+)/m(O^+)\right]^{1/2}$. The contour levels decrease successively by a factor $e^{1/2}$ rom the maximum.

We have therefore chosen to use one set of boundary conditions to the model, which we will compare with all data.

To study the effect of WPI (altitude-dependent and velocity-dependent) on O^+ ions, we compute the ion velocity distribution function $f(O^+)$ at several altitudes in the

simulation region and for different values of $\lambda_\perp$. The simulations of O^+ ions velocity distribution function $f(O^+)$ are shown in Fig. 2. For the case ($\lambda_\perp \to \infty$) i.e. $k_\perp \to 0$, the diffusion coefficient ($D_\perp$) becomes altitude dependent and velocity independent according to Eq. (6). The distribution function $f(O^+)$ at 1.7 R_E is Maxwellian and consistent with the assumed boundary conditions. As geocentric altitude increases, the diffusion coefficient $D_\perp(O^+)$ increases, according to Eq. (5), then the role of WPI becomes significant in heating the ions in the perpendicular direction (i.e. the strength of WPI increases), the resulting perpendicular heating leads to the formation of "pancake-like" distributions $[T_\perp(O^+) > T_\parallel(O^+)]$, which folds into O^+ conics due to the effect of mirror force. For the case of ($\lambda_\perp = 50$ km), the behavior of ions remains the same as the case of $\lambda_\perp \to \infty$, up to 7.0 R_E, the toroidal features start to appear at 7.34 R_E, become obvious at 8.69 R_E, and saturate above that altitude. The toroidal features appear when the finite wavelength of the electric field turbulence limits the velocity diffusion for particles with a gyroradius comparable to the wavelength. The formation of ion toroids can be explained in terms of the expression of the diffusion coefficient ($D_\perp$). According to Eq. (6), $D_\perp(r, v_\perp)$ has a maximum value near zero perpendicular velocity (i.e. $v_\perp \approx 0$) (i.e. $(k_\perp v_\perp / \Omega) < 1$), and decreases rapidly for large values of $v_\perp$ (i.e. $k_\perp v_\perp / \Omega \geq 1$); therefore, the ions ($H^+$ or O^+) tend to move out of the region of large diffusion coefficient $D_\perp$ (i.e. $k_\perp v_\perp / \Omega < 1$) and accumulate in region of relatively low diffusion coefficient $D_\perp$ (i.e. $k_\perp v_\perp / \Omega \geq 1$), forming the aforementioned toroidal distribution. For shorter wavelengths of the electric field turbulence, this occurs at progressively lower altitudes. It will also affect O^+ at a lower altitude than H^+ because of the larger gyroradius of O^+ for a given perpendicular velocity.

For the case ($\lambda_\perp = 20$ km), the distribution functions behaves as in the case of ($\lambda_\perp \to \infty$) and ($\lambda_\perp = 50$ km) up to ($\sim$5.97 R_E), but the toroidal features appear at a lower altitudes (i.e. $\sim$6.66 R_E), they are well established at ($\sim$7 R_E), and saturate above that altitude. However, for the case ($\lambda_\perp = 8$ km), the toroidal shape appears at lower altitudes, it starts to appear at altitude ($\sim$5.97 R_E) and becomes well established at altitude ($\sim$6.66 R_E). Moreover, for the case ($\lambda_\perp = 1$ km) the toroidal features appear at lower altitude ($\sim$4.27 R_E), become obvious at 5.29 R_E, and the distribution function $f(O^+)$becomes saturated above 5.29 R_E.

For the cases ($\lambda_\perp = 50$ km, $\lambda_\perp = 20$ km, $\lambda_\perp = 8$ km, and $\lambda_\perp = 1$ km), the O^+ velocity distribution function $f(O^+)$ saturates after forming the toroidal shape, because the effect of WPI becomes negligible and the perpendicular heating turns to be self-limiting. In other words, as $\lambda_\perp$ decreases, the argument $k_\perp v_\perp / \Omega$ or the ratio of the ion gyroradius to the wavelength $\lambda_\perp$ approaches one at lower altitudes and consequently, the toroids appear at these altitudes, namely for the case ($\lambda_\perp = 1$ km) the toroids appear at 4.27 R_E, and become well established at 5.29 R_E.

Figure 3 presents the altitude profiles of lower order moments of O^+ ions. The drift velocity (top-right panel) of O^+ ions $u(O^+)$ increases with altitude for all $\lambda_\perp$, because the role of WPI is to heat the ions in the perpendicular direction, part of this gained energy due to heating process transfer from the perpendicular direction to the parallel direction due to the mirror force, thus the acceleration of the ions in the upward direction will be increasesd. However, we note that the drift velocities at low altitudes (i.e. below 4.5 R_E) are the same for different values of $\lambda_\perp$, since the argument $k_\perp v_\perp / \Omega$ is less than unity (i.e. the behavior of O^+ ions below that altitude (4.5 R_E) is the same for all values of $\lambda_\perp$). For the case ($\lambda_\perp = 50$ km), the acceleration rate decreases, the drift velocity uO^+ still increasing but with a smaller rate above the saturation point which occurs at 7.5 R_E. For the case ($\lambda_\perp = 20$ km), we see that the saturation appears earlier at 6.5 R_E, for the case ($\lambda_\perp = 8$ km), the saturation appears at lower altitude ($\sim$6.0 R_E), for the case ($\lambda_\perp = 1$ km), $u(O^+)$ is reduced more and more and the saturation appears at 4.5 R_E. These results have a close agreement with the velocity distribution functions displayed in Fig. 2.

The drift velocity $u(O^+)$ still increases but with a smaller rate as $\lambda_\perp$ decreases, because of the reduction in the heating rate. This can be explained as follows: the expression for the diffusion coefficient ($D_\perp$) is a function of altitude and velocity as shown in Eq. (6). As $\lambda_\perp$ decreases, the expression $(k_\perp v_\perp / \Omega)^{-3}$ decreases, so the diffusion coefficient ($D_\perp$) decreases, thus the strength of WPI decreases and the heating process becomes negligible. However, below the saturation points mentioned above, the effect of WPI is the same; in other words, it is independent of $\lambda_\perp$, i.e. below the saturation points the effect of velocity dependent WPI is negligible and the main contribution to the heating process is coming from the altitude-dependent part of the diffusion coefficient. Since O^+ ions are in the flux-limiting flow condition (Barakat and Schunk, 1983), a corresponding increase in the ions density is expected to compensate the decrease in the ions drift velocity, and hence to keep the net escape flux constant.

The lower left panel of Fig. 3 presents O^+ ions perpendicular temperature. The behavior of this $T_\perp(O^+)$ is due to the effect of WPI that heats O^+ ions in the perpendicular direction, and to the effect of perpendicular adiabatic cooling, in which part of the energy is transferred from perpendicular direction to the parallel direction in order to keep the first adiabatic invariant μ constant (i.e. $\mu = mv^2/2B$). As altitude increases, $T_\perp(O^+)$ increases due to the effect of WPI that dominates the effect of perpendicular adiabatic cooling. Also, it is clear from the altitude profile of O^+ ions perpendicular temperature that as $\lambda_\perp$ decreases $T_\perp(O^+)$ decreases, because $D_\perp$ decreases, and consequently the heating rate decreases. At lower altitudes the heating is enhanced owing to the pressure cooker effect (Barakat and Barghouthi, 1994), which results from the temporary trapping of O^+ ions between the lower magnetic deflection point and the upper gravitational point (see Fig. 1), when an ion bounces between these two

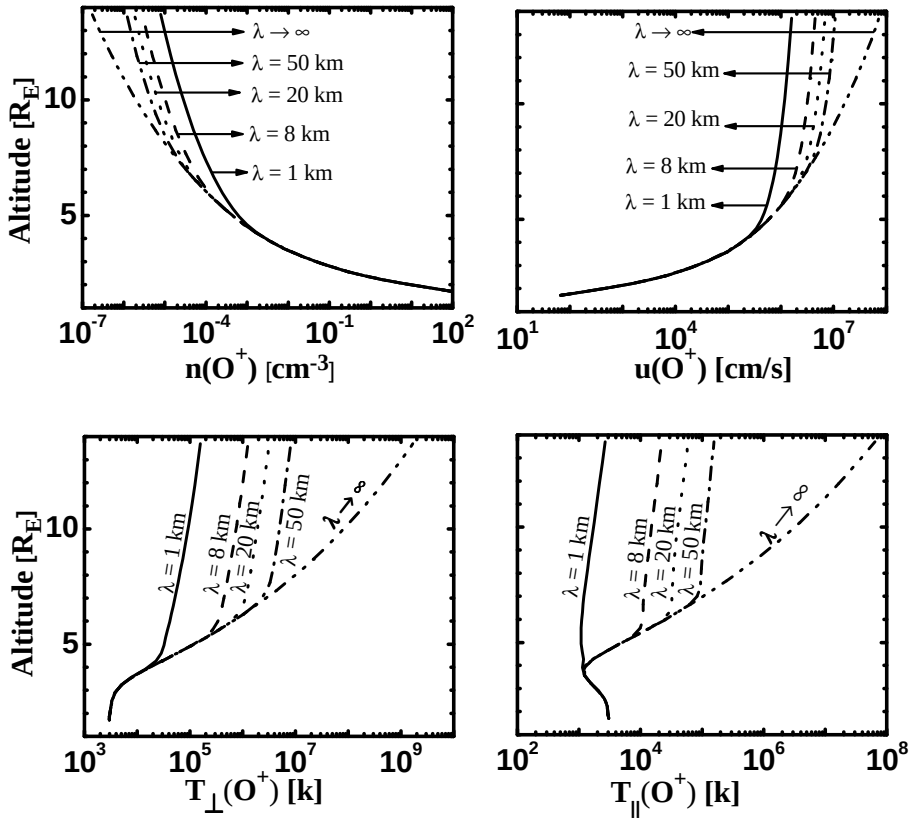

Fig. 3. Altitude profiles of the lower order O^+ moment for different electromagnetic turbulence wavelengths ($\lambda_\perp$). The wavelengths considered here are $\lambda_\perp \to \infty$ (double-dotted dashed line), $\lambda_\perp = 50$ km (dotted dashed line), $\lambda_\perp = 20$ km (dotted line), $\lambda_\perp = 8$ km (dashed line), $\lambda_\perp = 1$ km (solid line). The O^+ moments considered here are: density $n(O^+)$ (top left), drift velocity $u(O^+)$ (top right), perpendicular temperature $T_\perp(O^+)$ (bottom left), and parallel temperature $T_\parallel(O^+)$ (bottom right).

deflection points, it gains more and more energy due to WPI and then its perpendicular temperature increases. This increases transport times, and thus the distance the flux tube will drift in the perpendicular direction at the time an ion has reached a given altitude.

The profiles of O^+ ions parallel temperature $T_\parallel(O^+)$ is influenced by WPI, because as O^+ ions perpendicular temperature increases due to WPI, part of this energy is transferred from the perpendicular direction to the parallel direction, and consequently, the parallel temperature increases at high altitudes. At low altitudes O^+ ions parallel temperature $T_\parallel(O^+)$ decreases, owing to parallel adiabatic cooling (Barakat and Lemaire, 1990) in which the WPI heats the ions in the perpendicular direction and then part of this energy is transferred to the parallel direction which enhances O^+ ions drift velocity, and consequently parallel temperature decreases as shown in Eq. (9). One should note when comparing parallel temperatures of models and observations that observed parallel temperatures can be affected by temporal variations in addition to the energy transfer through the mirror force which is described by the model. Therefore, a larger parallel temperature in the observations than in the model need not be a major problem for the model, it may just reflect temporal variations of the heating process. The most important features are rather the altitude profiles of the perpendicular temperature and the parallel velocity. Density profiles, though important to reproduce accurately, are mainly a function of boundary conditions and the drift velocity profile.

Figure 4 shows the simulation results of H^+ ions velocity distribution functions $f(H^+)$. It is clear that the velocity distribution is Maxwellian at the lower boundary (i.e. 1.7 R_E) and this is consistent with the assumed initial conditions. At 5.29 R_E, the width of the velocity distribution function in the perpendicular direction is less than the width in the parallel direction, in other words as altitude increases perpendicular temperature decreases and parallel temperature increases i.e. $T_\parallel(H^+) > T_\perp(H^+)$. This is due to the effect of perpendicular adiabatic cooling in which part of energy is transfer from perpendicular direction to the parallel direction in order to keep the first adiabatic invariant constant. At 8.19 R_E, the heating rate in the perpendicular direction due to WPI increases and dominates the effect of perpendicular adiabatic cooling, i.e. $T_\perp(H^+) > T_\parallel(H^+)$.

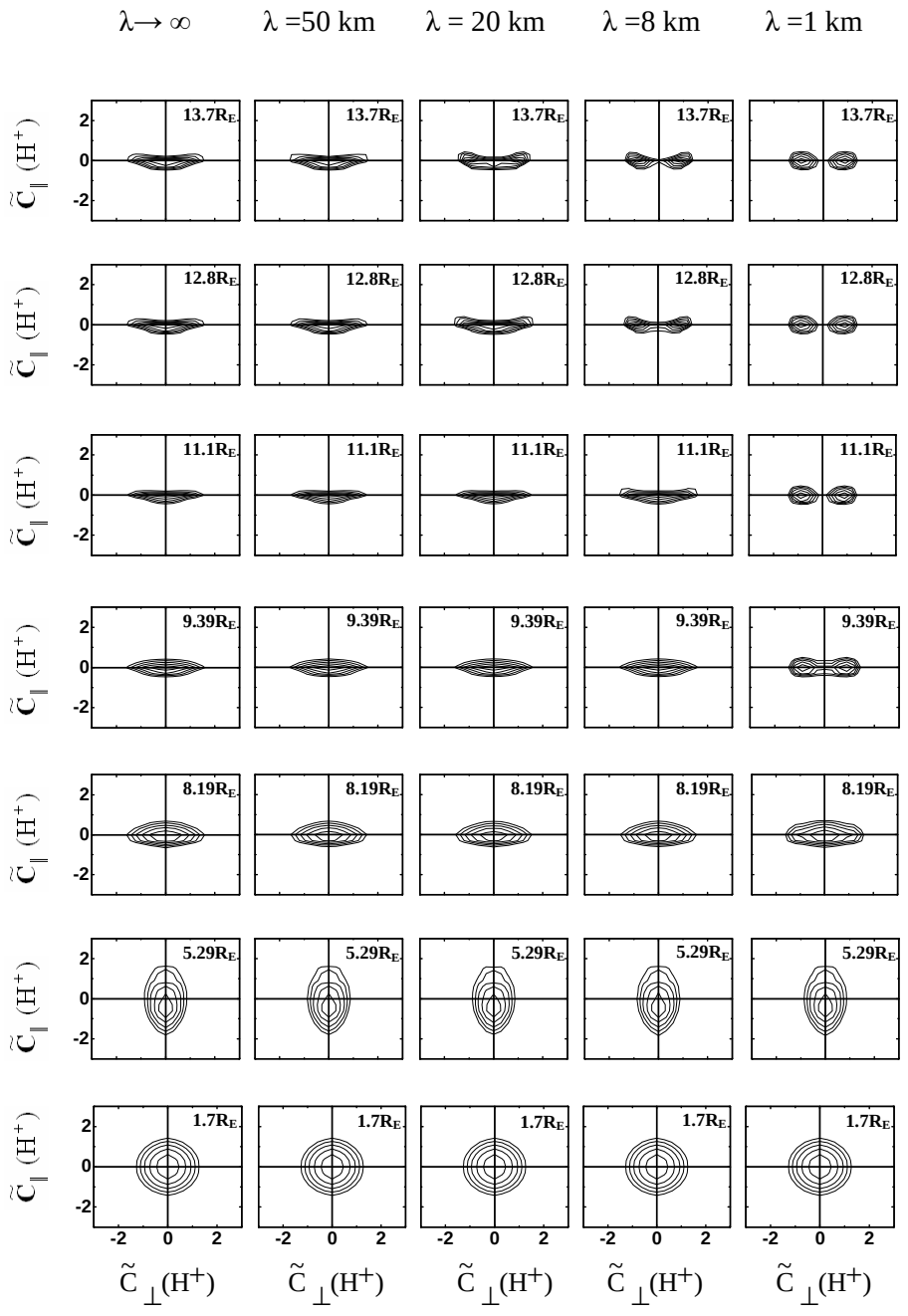

Fig. 4. H^+ ions velocity distribution functions at different geocentric distances (1.7, 5.29, 8.19, 9.39, 11.1, 12.8, and 13.7 R_E) for different electromagnetic turbulence wavelengths ($\lambda_\perp$), the wavelengths considered here are $\lambda_\perp \to \infty$ (1st panel), $\lambda_\perp = 50$ km (2nd panel), $\lambda_\perp =$ 20 km (3rd panel), $\lambda_\perp = 8$ km (4th panel), and $\lambda_\perp = 1$ km (5th panel). $f(H^+)$ is represented by equal values contours in the normalized velocity $(\tilde{c}_{||}, \tilde{c}_\perp)$ plane, where$\tilde{c} = \left[v - u(H^+)\right] / \left[2kT(H^+)/m(H^+)\right]^{1/2}$. The contour levels decrease successively by a factor $e^{1/2}$ from the maximum.

To be specific, for the case ($\lambda_\perp \to \infty$), the distribution function is Maxwellian at the lower boundary. As geocentric altitude increases, the diffusion coefficient $D_\perp(H^+)$ increases, which means that the heating rate increases and consequently the perpendicular temperature increases. Initially, the effect of perpendicular adiabatic cooling is dominant, i.e. the energy transfer from perpendicular direction to the parallel direction in order to keep the first adiabatic invariant constant is larger than the gain due to WPI. Therefore, perpendicular temperature decreases in the altitude range (1.7 R_E to 5 R_E), and consequently the velocity distribution $f(H^+)$ develops large temperature anisotropy $[T_\parallel(H^+) > T_\perp(H^+)]$,

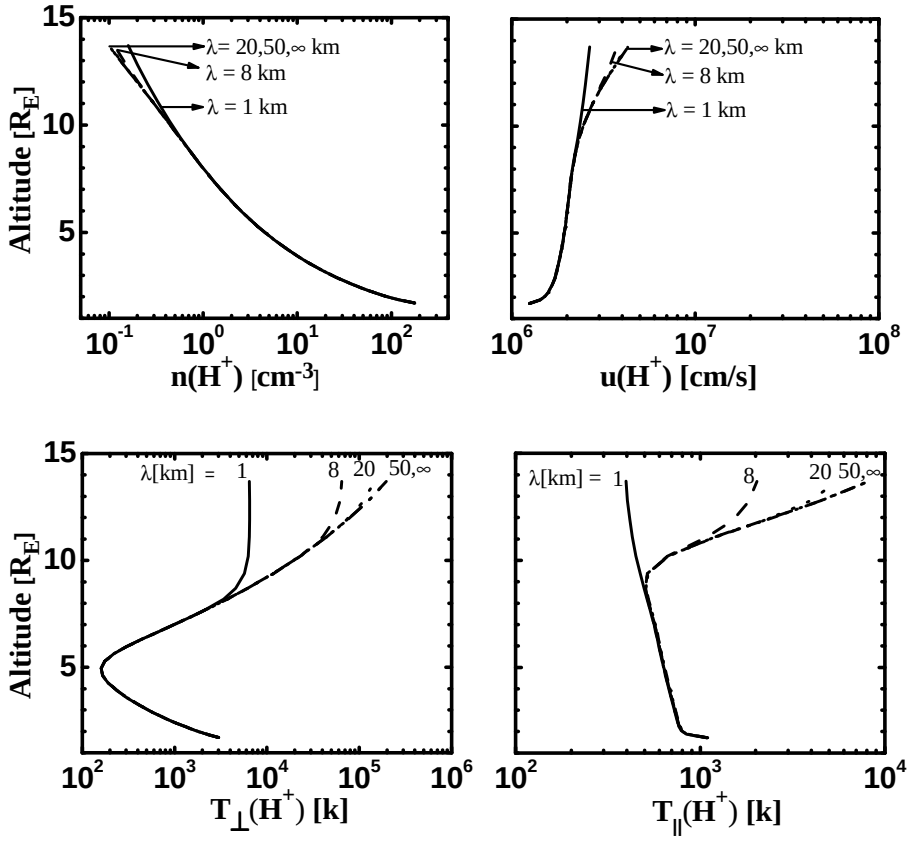

Fig. 5. Altitude profiles of the lower order H^+ moment for different electromagnetic turbulence wavelengths ($\lambda_\perp$). The wavelengths considered here are $\lambda_\perp \to \infty$ (double-dotted dashed line), $\lambda_\perp = 50$ km (dotted dashed line), $\lambda_\perp = 20$ km (dotted line), $\lambda_\perp = 8$ km (dashed line), $\lambda_\perp = 1$ km (solid line). The H^+ moments considered here are: density $n(H^+)$ (top left), drift velocity $u(H^+)$ (top right), perpendicular temperature $T_\perp(H^+)$ (bottom left), and parallel temperature $T_\parallel(H^+)$ (bottom right).

but at 8.19 R_E the temperature anisotropy is inverted [i.e. $T_\perp(H^+) > T_\parallel(H^+)$] because the effect of WPI increases with altitude and dominates the effect of perpendicular adiabatic cooling. At higher altitudes, the role of WPI becomes significant and this yields H^+ conics at geocentric altitude 9.38 R_E, which become obvious at 11.1 R_E, and above this altitude the conics features are saturated. Also, for the case ($\lambda_\perp = 50$ km) the velocity distribution function remains the same as for the case ($\lambda_\perp \to \infty$) at all geocentric altitudes, this means that the contribution of the velocity part in the diffusion coefficient is negligible and still $D_\perp$ is velocity independent. This is consistent with the smaller gyroradius of H^+ as compared to O^+.

For the case ($\lambda_\perp = 20$ km), the velocity distribution function remains the same as the cases ($\lambda_\perp \to \infty$) and ($\lambda_\perp = 50$ km) up to 12.8 R_E, but at 13.7 R_E the distribution function begins to display toroidal features. For the case ($\lambda_\perp = 8$ km), the distribution function remains the same as the cases ($\lambda_\perp \to \infty$), ($\lambda_\perp = 50$ km), and ($\lambda_\perp = 20$ km) up to ($\sim$11.1 R_E), but at 12.8 R_E the distribution function starts to display toroidal features, which become obvious at 13.7 R_E. Moreover, for the case ($\lambda_\perp = 1$ km), the toroidal features appear at a lower altitude ($\sim$9.39 R_E), and become more pronounced at geocentric altitude ($\sim$11.1 R_E).

Figure 5 shows the altitude profiles for H^+ lower order moments for wide range of $\lambda_\perp$. The drift velocity of H^+ ions $u(H^+)$ increases with altitude, owing to the effect of WPI and its role in heating the ions in perpendicular direction. The case ($\lambda_\perp = 50$ km) is similar to the case of ($\lambda_\perp \to \infty$), where the two cases are the same for all altitudes in the simulation tube. But for the case ($\lambda_\perp = 20$ km), the heating rate decreases, and so drift velocity $u(H^+)$ is reduced more and more above the saturation point which occurs at 12.0 R_E. For the case ($\lambda_\perp = 8$ km), the saturation point appears at 10.5 R_E. For the case ($\lambda_\perp = 1$ km), $u(H^+)$ is reduced more and more and the saturation point occurs at lower altitude i.e. 7.8 R_E. The drift velocity $u(H^+)$ decreases as $\lambda_\perp$ decreases, because of the reduction of the heating rate. The density of H^+ ions $n(H^+)$ increases as $\lambda_\perp$ decreases to keep the escape flux constant.

The behavior of H^+ ions perpendicular temperature $T_\perp(H^+)$ at altitudes above 5 R_E is increasing monotonically

with altitude, since the effect WPI is greater than that of perpendicular adiabatic cooling (i.e. WPI is dominant). But at lower altitudes $T_{\perp}(H^+)$ is decreasing with altitude, since the perpendicular adiabatic cooling effect dominates the effect of WPI.

As a result of WPI, H^+ ions are energized through heating in the perpendicular direction, part of this energy is transferred to the parallel direction, and consequently, the parallel temperature increases at high altitudes, but at lower altitude H^+ ions parallel temperature $T_{\parallel}(H^+)$ decreases, since the parallel adiabatic cooling (Barakat and Lemaire, 1990) is dominant and the effect of WPI is weak. On the other hand, at relatively intermediate altitudes the effect of WPI is strengthened, but parallel adiabatic cooling is still dominant; therefore, H^+ ions parallel temperature $T_{\parallel}(H^+)$ decreases slowly with altitude.

4 Comparison between simulation results and observations

Barghouthi (2008) compared between the simulation result of Barghouthi model for H^+ and O^+ ions outflows in the auroral region with the corresponding observations, he found an excellent agreement, in particular when the characteristic perpendicular wavelength of the electromagnetic turbulence was 8 km. Also, according to comparison between the simulation results of the polar wind for different wavelengths, we find a general agreement with the corresponding observations for this wavelength, therefore we choose to present the comparison for the case when $\lambda_{\perp} = 8$ km. In this paper, we searched the literature and looked for different observations related to the polar wind over the range from 1.7 R_E to 13.7 R_E. We found observations concerning density, velocity, parallel velocity, perpendicular temperature, parallel temperature, temperature, energy, and temperature anisotropy ($T_{\parallel} / T_{\perp}$), for both H^+ and O^+ ions and at different altitudes. Therefore, for the sake of comparison, we have computed from the simulation results presented in Sect. 3, the following: lower order moments (i.e. density, drift velocity, perpendicular and parallel temperatures for both ions (Fig. 6), temperatures for both ions (Fig. 7), and H^+ and O^+ temperature anisotopies ($T_{\parallel} / T_{\perp}$) (Fig. 8). We have used these figures either to obtain numerical values or to investigate the qualitative behavior of ion outflows.

4.1 Quantitative comparison

In this sub-section, we compare between the observations and simulation results of Barghouthi model quantitativly, the comparisons are tabulated in Table 1 for H^+ ions, and Table 2 for O^+ ions. We will compare a fixed model with both statistical and case studies of the polar wind. This will affect the comparison in a number of ways which we will discuss below.

First of all we have used a fixed set of lower boundary conditions. If wave-particle interaction during the transport path is dominant, the lower boundary conditions will not be so important for the shape of the ion distributions at high altitude. Due to the action of the mirror force almost all initial energy will have been turned into parallel energy, so that the boundary conditions mainly affect the parallel bulk velocity at high altitude. The effect of the boundary conditions is by far most important for the number flux and density, which will be totally determined by the boundary conditions if all other parameters are kept constant. Therefore, absolute values of density and number flux are less important for our comparison, while shape of the distribution functions and altitude profiles of all parameters are important. Comparison with statistical studies makes most sense for an average model. For case studies one should in principle adjust both heating rates and lower boundary conditions to those corresponding to the time of measurements. We have chosen to include some case studies anyway, to see how they fit into our general model, to illustrate the range of different observations that exist. Before discussing the quantitative and qualitative comparisons between simulations and corresponding results, it is important to note, in observational studies they use the terms velocity, parallel velocity, and drift velocity. All these terms are the same in observational studies and correspond to drift velocity in simulation studies.

Table 1, Figs. 6, 7, and 8 present a comparison between H^+ observations with the corresponding simulation results obtained by Barghouthi model. We find three levels of agreement:

1. Very close agreement, for example, H^+ parallel velocity at 4.17 R_E, H^+ perpendicular temperature at 1.79 R_E, and H^+ parallel velocity at altitudes around 2.3 R_E.

2. The simulation results are in the range of observations, for example, H^+ density at 9.0 R_E, H^+ velocity at 2.0 R_E, H^+ parallel velocity at 1.79 R_E and 9.0 R_E, and H^+ temperature at 2.0 R_E.

3. In the same order, i.e. good agremeent, for example, H^+ parallel temperature at 1.79 R_E , H^+ perpendicular temperature at 9.0 R_E, and H^+ density at 4.17 R_E.

We also note that the Barghouthi model results are consistent with the observations of Engwall et al. (2009), in terms of our parallel velocities of about 20–30 km s^{-1} at 10–14 R_E. Furthermore the wake effect used by Engwall et al. (2009) exists when the thermal energy is smaller than the drift energy which is in turn smaller than the spacecraft potential which can reach several tens of volts for a sunlit spacecraft in the lobes. This is consistent with the low H^+ temperatures predicted by Barghouthi model. We note also that Nilsson et al. (2010) concluded that there was room for very little additional acceleration in the lobes apart from the relatively small centrifugal acceleration. This may mean that wave activity in

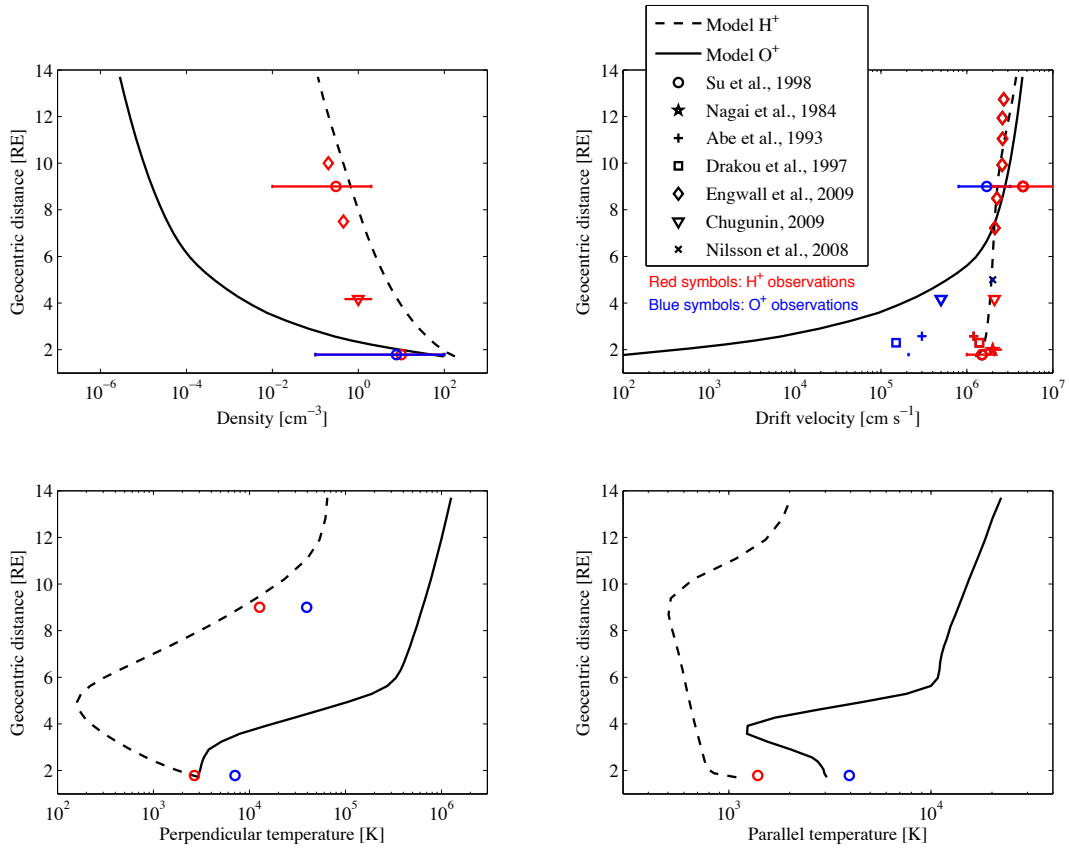

Fig. 6. Altitude profiles of the lower order moment for O^+ ions (solid line) and H^+ ions (dashed line) when $\lambda_\perp = 8$ km. The moments considered here are: density $n\left[\mathrm{cm}^{-3}\right]$ (top left), drift velocity $u\left[\mathrm{cm}^{-3}\right]$ (top right), perpendicular temperature $T_\perp[k]$ (bottom left), and parallel temperature $T_\parallel[k]$ (bottom right). Different corresponding observations are marked on the profiles.

the lobes is less than in Barghouthi model and that revised velocity diffusion coefficients may be needed for the conditions described in the observations of Engwall et al. (2009).

We also find some discrepancies, mainly related to the H^+ perpendicular to parallel temperature ratio (Fig. 8), which is above unity at low (i.e. below 2 R_E) and high (i.e. above 6 R_E) altitudes and less than unity at intermediate (i.e. 2–6 R_E) altitudes, however it is below than unity in Su et al. (1998) observations.

Table 2, Figs. 6, 7, and 8 present a comparison between O^+ observations with the corresponding simulations obtained by Barghouthi model, also we find three levels of agreement, they are:

1. Very close agreement, for example, O^+ parallel temperature at 1.79 R_E, O^+ velocity at 5.0 R_E, and O^+ temperature at 4.17 R_E.

2. The simulation results are in the range of obsevations, for example, O^+ density at 1.79 R_E, O^+ parallel velocity at 9.0 R_E, and O^+ temperature in the range 2.1 R_E–2.58 R_E.

3. In the same order, i.e. good agreement, for example, O^+ temperature anisotropy at 1.79 R_E, O^+ perpendicular temperature at 1.79 R_E, and O^+ parallel velocity at 4.17 R_E.

We also find some notable disagreements. These are:

1. The O^+ density at 9.0 R_E is much lower in the model than in the observations of Su et al. (1998), about three orders of magnitude too small.

2. The O^+ perpendicular temperature is much higher in the model than in the observations of Su et al. (1998) at 9.0 R_E, 52 eV as compared to an average of just 3.4 (with a typical range of 0.35–22 in the measurements).

3. The O^+ perpendicular to parallel temperature ratio is far too high in the model (about 50) as compared to just 0.54 in the Su at al. (1998) observations at 9.0 R_E.

4. $T_\perp(O^+)/T_\perp(H^+)$ is equal to 3.43 at 9.0 R_E (Su et al., 1998); however, in this study it is 2 order of magnitude larger.

Table 1. Comparison between the observations and simulation results of Barghouthi model for H^+ ions. Please note, in observational studies they use the terms velocity, parallel velocity, and drift velocity. All these terms are the same in observational studies and correspond to drift velocity in simulation studies.

Altitude (R_E) H^+ ions	Characteristics	Barghouthi model predictions	Observations
1.79 R_E	Density n (cm^{-3})	100	(0.1–100) (Su et al., 1998)
9.0 R_E	Density n (cm^{-3})	0.7	(0.01–2, and its average was 0.3) (Su et al., 1998)
4.17 R_E	Density n (cm^{-3})	∼4	0.5–2 (Chugunin, 2009)
2.0 R_E	Drift velocity v ($km\,s^{-1}$)	16.1	(16–25) (Nagai et al., 1984)
2.58 R_E	Velocity v ($km\,s^{-1}$)	17.2	12 (Abe et al., 1993)
1.79 R_E	Parallel velocity $v_\parallel$ ($km\,s^{-1}$)	13.4	(10–21, and its average was 15) (Su et al., 1998)
4.17 R_E	Parallel velocity $v_\parallel$ ($km\,s^{-1}$)	20	21 (Chugunin, 2009)
∼2.3 R_E	Parallel velocity $v_\parallel$ ($km\,s^{-1}$)	16.1	14 (Drakou et al., 1997)
9.0 R_E	Parallel velocity $v_\parallel$ ($km\,s^{-1}$)	22.8	(20–110, and its average was 45) (Su et al., 1998)
1.79 R_E	Perpendicular temperature $T_\perp$ (eV)	0.22	0.23 (Su et al., 1998)
9.0 R_E	Perpendicular temperature $T_\perp$ (eV)	0.7	1.1 (Su et al., 1998)
1.79 R_E	Parallel temperature $T_\parallel$ (eV)	0.082	0.12 (Su et al., 1998)
2.0 R_E	Temperature T (eV)	0.15	0.12–0.2) (Nagai et al., 1984))
2.1 R_E–2.58 R_E	Temperature T (eV)	(0.11–0.07)	(0.05–0.35) (Drakou et al., 1997; Su et al., 1998)
1.78 R_E	$T_\parallel/T_\perp$	0.4	0.52 (Su et al., 1998)

5. $n(O^+)/n(H^+)$ 9.0 R_E is in the range 0.016–1, with an average value of 0.156 (Su et al., 1998); however, in this study it is of order of 10^{-5}.

From these comparisons, we can say that the simulation results obtained by Barghouthi model are close to many of the corresponding observations at different altitudes for H^+, whereas some improvements are needed for O^+. We believe the improvements needed for O^+ are mainly related to the number flux at the lower boundary. As our densities at low altitude are in good agreement with observations, the number flux must be increased with a higher drift velocity. This will mainly affect the velocities at low altitude, whereas as the initial velocity becomes negligible the initial number flux will mainly affect the densities at high altitude. We also note that such a higher number flux than the value provided using Polar data as boundary condition is consistent with a cleft ion fountain source for the O^+ ions. Furthermore we will need to look into the magnitude of the heating of O^+ if the values reported by Su et al. (1998) are typical.

4.2 Qualitative comparison

In addition to the above numerical comparisons, we compare between the qualitative behavior of the ions outflows in the polar wind with different observations. The comparisons are summarized in Table 3. Similarly, from the corresponding comparisons shown in Table 3, we can conclude that the qualitative behavior of H^+ ions and many properties of the O^+ ions in the polar wind are close to the observations at different altitudes and for both ions. The list is relatively self-described, so we only providde a very brief summary here: the model reproduces the gross features that the ion velocity increases with altitude and is supersonic at high altitude,

Table 2. Comparison between the observations and simulation results of Barghouthi model for O^+ ions. Please note, in observational studies they use the terms velocity, parallel velocity, and drift velocity. All these terms are the same in observational studies and correspond to drift velocity in simulation studies.

Altitude (R_E) O^+ ions	Characteristics	Barghouthi model predictions	Observations
1.79 R_E	Density n (cm^{-3})	30	(0.1–100, and its average was 7.7) (Su et al., 1998)
5.0 R_E	Velocity v ($km\,s^{-1}$)	15	20 (Nilsson et al., 2008)
4.17 R_E	Parallel velocity $v_\parallel$ ($km\,s^{-1}$)	2	5 (Chugunin, 2009)
9.0 R_E	Parallel velocity $v_\parallel$ ($km\,s^{-1}$)	27.5	(8–32, and its average was 17), (Su et al., 1998)
1.79 R_E	Perpendicular temperature $T_\perp$ (eV)	0.28	0.61 (Su et al., 1998)
1.79 R_E	Parallel temperature $T_\parallel$ (eV)	0.28	0.34 (Su et al., 1998)
2.1 R_E–2.58 R_E	Temperature T (eV)	0.25	(0.05–0.35) (Drakou et al., 1997; Su et al., 1998)
4.17 R_E	Temperature T (K)	11 600	10 000 (Chugunin, 2009)
1.79 R_E	$T_\parallel/T_\perp$	0.95	0.55 (Su et al., 1998)
~8 R_E	Temperature (eV)	28	8 (Gurgiolo and Burch, 1982)

the density decreases and H^+ is the dominant species. O^+ is more energized than H^+ as seen both in a more rapidly increasing parallel velocity and higher temperatures.

It is very important to note that the simulation results obtained in this study (i.e. Sect. 3) have been used in the above comparisons and are computed by using the Barghouthi model with a fixed set of velocity diffusion coefficients (appropriate for the average polar wind); and we have used a set of typical boundary conditions for ions and electrons temperatures, ion drift velocities, and ion velocity distributions at the injection point. On the other side, the observations are conducted at different conditions: day side, night side, sometimes high and sometimes low geomagnetic activities, seasons, and many other ionospheric and magnetospheric conditions. Therefore, it is expected and accepted to have discrepancies between both results, but as soon as the model produces numerical simulations that are in the same order of the observations, and the simulated ion outflows have similar behavior to the observed ones, we have to modify the boundary conditions and to use the appropriate ones that have been measured in the same conditions that the observations have been observed and measured. Taking this into consideration, many of the discrepancies between the simulations and the observations either disappear or decrease. This study and another similar studies (e.g. Nilsson et al., 2010) are important because they try to explain the observations and to discuss the mechanism (mechanisms) that is (are) responsible for producing the observations, i.e. the physics behind the ion outflow behavior will be known and can be used to explain other observations that have been measured in similar conditions.

We finally note that Barghouthi model lacks one acceleration mechanism, the centrifugal acceleration (Horwitz et al., 1994), which has been experimentally estimated using Cluster data (Nilsson et al., 2008, 2010). For the cusp/mantle related outflow reported in Nilsson et al. (2008), the centrifugal acceleration added about 20–30 $km\,s^{-1}$ between 5 and 14 R_E. The centrifugal acceleration of cold ion outflow in the lobes was much less; for particles with initial parallel velocity of 20 $km\,s^{-1}$ at 5 R_E, the additional velocity at 14 R_E due to centrifugal acceleration would be about 5 $km\,s^{-1}$ (Nilsson et al., 2010, their Fig. 3). Low parallel velocities at low altitude will lead to long transport times for the polar wind plasma, which will most likely end up in the lobes rather than in the high altitude cusp/mantle. The cold, supersonic plasma discussed in Nilsson et al. (2010) agree with the prediction of the Barghouthi model and with other polar wind observations, whereas the cusp/polar cap proton population reported in Nilsson et al. (2008) is mainly of magnetosheath origin. Omission of the centrifugal acceleration will therefore not have a strong impact on the final result of the model.

Table 3. Comparison between Barghouthi model predictions and experimental verifications. Please note, in observational studies they use the terms velocity, parallel velocity, and drift velocity. All these terms are the same in observational studies and correspond to drift velocity in simulation studies.

Experimental verifications	Barghouthi model predictions
1. The polar wind dominated by H^+ ions at 9 R_E (Su et al., 1998).	The densities of O^+ and H^+ ions at 9 R_E are equal to 1.6×10^{-5} and 0.7 cm^{-3}, respectively, as shown in Fig. 6. Therefore, at this altitude H^+ ion is the dominated species.
2. O^+ density was an order of magnitude smaller than the H^+ density in the geocentric altitude (5.5–8.9 R_E) (Elliott et al., 2001)	O^+ density is much smaller than H^+ density in the altitude range (5.5–8.9 R_E), as shown in Fig. 6.
3. At very high altitudes (above ∼9 R_E), the polar wind ions have large velocities (Su et al., 1998)	At 9 R_E, the velocities of O^+ and H^+ ions are 30 and 20 km s^{-1}, respectively, also at 13.7 R_E these velocities are 45 and 32 km s^{-1}, respectively (Fig. 6).
4. As polar wind ions flow upward, an increase in drift speed of the polar wind ions observed (Yau et al., 2007)	The drift velocity of O^+ ions increases with altitude as shown in Fig. 6.
5. Compared with H^+ ions, O^+ ions attain significant average upward velocity at higher altitudes (Abe et al., 1993).	Compared with H^+ ions, O^+ drift velocity increases very dramatically with altitude as shown in Fig. 6
6. Polar wind ion velocity increases linearly with geocentric distance over the altitude range (2.1 to 4.66 R_E) (Persoon et al., 1983)	According to Fig. 6, O^+ and H^+ velocities are, approximately, linearly increase with geocentric altitude in the range (2.1 to 4.66 R_E).
7. At altitude about 2 R_E outside the plasmasphere, the plasma density was typically below 10^3 cm^{-3} (Yau et al., 2007)	The densities of O^+ and H^+ ions at 2 R_E are 13 cm^{-3} and 100 cm^{-3}, respectively.
8. The polar wind plasma density was very low (typically <10 cm^{-3}) near 9 R_E (Moore and Delcourt, 1992)	The densities for O^+ and H^+ ions at 9 R_E are equal to 6×10^{-5} and 0.7 cm^{-3}, respectively.
9. In general, the velocity of O^+ ions increases with altitude above 2.03 R_E ,however for some geophysical conditions it may decrease at high altitudes (Abe et al., 2004)	The velocity of O^+ ions increases rapidly at low altitudes and increases slowly at high altitudes, as shown in Fig. 6.
10. The velocity of the polar wind ions increases with altitude (Drakou et al., 1997)	O^+ and H^+ velocities are increasing monotonically with altitude as shown in Fig. 6.
11. The polar wind ions are supersonic at 9 R_E (Su et al., 1998)	At 9 R_E, the velocities of O^+ and H^+ ions are 30 and 20 km s^{-1}, respectively, so they are supersonic at this altitude, since the thermal velocities of O^+ and H^+ ions are 2.16 and 8.62 km s^{-1} at the injection point, respectively.
12. At 1.8 R_E, H^+ ions are supersonic, while O^+ ions are subsonic (Su et al., 1998)	The velocities of O^+ and H^+ ions at 1.8 R_E are equal to 0.004 and 16 km s^-, respectively, so H^+ ions are supersonic, while O^+ ions are subsonic, since O^+ and H^+ thermal velocities are 2.16 and 8.62 km s^{-1} at the injection point, respectively.
13. The polar wind species were supersonic above 2.1 R_E (Drakou et al., 1997)	H^+ ions are supersonic above 1.8 R_E, and O^+ ions are supersonic above 4.0 R_E, as shown in Fig. 6.
14. The H^+ polar wind ion outflow is supersonic at high altitude (Nagai et al., 1984)	The velocity of H^+ ions equals to 15 km s^{-1} at 1.7 R_E and it increases with altitude. Therefore, H^+ ion outflow is supersonic flow above 1.7 R_E.
15. The averaged perpendicular to parallel temperature ratio for H^+ ions decreases with altitude in the range (1.79–1.95 R_E) (Su et al., 1998)	The perpendicular to parallel temperature ratio for H^+ ions decreases with altitude in the range (1.7 - 5 R_E), as shown in Fig. 8.
16. O^+/H^+ parallel temperature ratio, $< T// (O^+)/T// (H^+) > \sim 4.6$ at 1.87 R_E (Su et al., 1998)	O^+/H^+ parallel temperature ratio, $< T// (O^+)/T// (H^+) > \sim 3.52$ at 1.87 R_E.
17. O^+ ions have a higher temperature than the H^+ ions in both the parallel and perpendicular directions (Su et al., 1998)	The parallel and perpendicular temperatures of O^+ ions are greater than that of H^+ ions at all altitudes, as shown in Fig. 6.
18. The perpendicular temperature exceeds the parallel temperature for H^+ ions at 1.8 R_E (Su et al., 1998)	The parallel and perpendicular temperatures of H^+ ions at 1.8 R_E are 1100 and 3000 k, respectively.
19. O^+ ions have a higher temperature than H^+ ions, at 1.8 and 9 R_E (Su et al., 1998)	The temperatures of O^+ and H^+ ions at 1.8 R_E are equal to 0.26 and 0.18 eV, respectively, and at 9 R_E are equal to 36 eV and 0.5 eV, respectively; therefore, the temperature of O^+ ions exceeds the temperature of H^+ ions at both altitudes, as shown in Fig. 6.
20. $T///T\perp > 1$ at 4.17 R_E for H^+ ions, when there is no heating (Chugunin, 2009).	$T///T\perp > 1$ at 4.17 R_E for H^+ ions (Fig. 8), the effect of WPI on H^+ ions is negligible below this altitude.

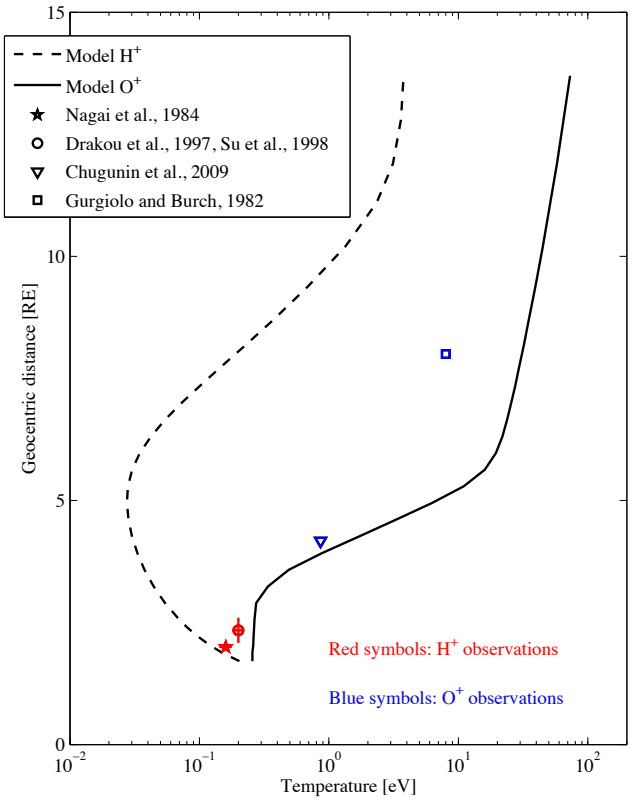

Fig. 7. Altitude profiles of ions temperatures, for O^+ ions (solid line) and H^+ ions (dashed line), when perpendicular wavelength of the electromagnetic turbulence $\lambda_\perp = 8$ km. Different corresponding observations are marked on the profiles.

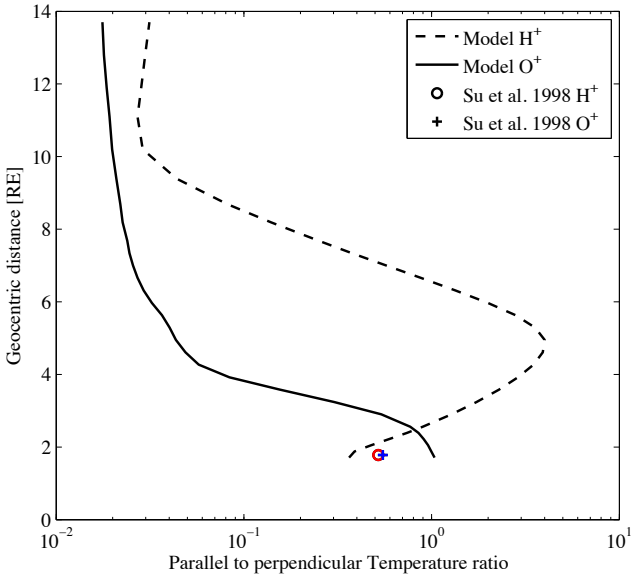

Fig. 8. Altitude profiles of ions temperature anisotropy ($T_\parallel / T_\perp$), for O^+ ions (solid line) and H^+ ions (dashed line), when perpendicular wavelength of the electromagnetic turbulence $\lambda_\perp = 8$ km. Different corresponding observations are marked on the profiles.

5 Discussions and conclusions

The Barghouthi model was used to simulate the effect of wave-particle interactions (i.e. altitude and velocity dependent) on H^+ and O^+ ions outflows at high-altitudes and high-latitudes in the polar wind region. This model also includes the effects of gravity, polarization electrostatic field, and the divergence of the geomagnetic field lines of the Earth. The only major accleration mechanisms left out are the centrifugal acceleration mechanism (Northrop, 1963), and the effect of photoelectrons (Su et al., 1998). The effects of wave-particle interactions (in which the ions get heated in the perpendicular direction and part of the gained energy transfer to the parallel direction owing to the conservation of the first adiabatic invariant) on H^+ and O^+ ions outflows was modeled. Because of the dependence of wave-particle interactions on the velocity diffusion coefficient $D_\perp(r, v_\perp)$, we developed a form for this coefficient as a function of position (r / R_E) along geomagnetic field lines of the Earth and injected ion perpendicular velocity $(v_\perp)$. As shown in Eq. (6), the diffusion coefficient depends on the perpendicular wavelength of the electromagnetic turbulence $\lambda_\perp$. This $\lambda_\perp$ has been included in the model as a parameter, thus in the simulation we considered the following values: [$\lambda_\perp = \infty$, 50, 20, 8, and 1 km]. From the polar wind simulations we have found the following:

1. The temperature anisotropy $(T_\perp / T_\parallel)$ for H^+ ions is reduced at lower altitudes, and it is reversed at higher altitudes, because the effect of perpendicular adiabatic cooling dominated the effect of wave-particle interactions at low altitudes since the heating rate is very weak. However, at higher altitudes the heating rate becomes strong and consequently the heating process overcomes the effect of perpendicular adiabatic cooling. This is not in full agreement with some observations, so the heating at high altitude may be overestimated in the model. On the other hand, the temperature anisotropy $(T_\perp / T_\parallel)$ for O^+ ions monotonically increases with altitude; this is due to the strength of wave-particle interactions that dominated other effects. The ratio is however too high as compared to observations. We argue that non-steady state situations will increase the range of parallel velocities of observed particles, so that in reality the parallel temperature is not solely determined by perpendicular heating and the mirror force as in the model, which can explain a part of the discrepancy, but likely not all. We note here that if the perpendicular temperature and parallel velocity are in good agreement with observations, then the total energy input into the ion population is also appropriately modeled.

2. The O^+ and H^+ ions velocity distribution functions [i.e. $f(O^+)$ and $f(H^+)$] develop conic features owing

to the effects of WPI (i.e. ion perpendicular heating) and the mirror force (i.e. diverging of geomagnetic field lines). The perpendicular temperature becomes greater than the parallel temperature. O^+ ions first develop conic features at ($\sim$4.27 R_E), while H^+ ions first develop conic features at ($\sim$11.1 R_E) for the case when the perpendicular wavelength of the electromagnetic turbulence $\lambda_\perp = 8$ km.

3. O^+ ions are preferentially heated comparing with H^+ ions, where the temperature of O^+ ions is higher than that of H^+ ions at all altitudes. This is owing to the potential energy of H^+ ions: it is negative and decreasing with altitude, while O^+ potential energy is positive and monotonically increasing with altitude. In addition, the diffusion coefficient of O^+ ions $D_\perp(O^+)$ is greater than the diffusion coefficient of H^+ ions $D_\perp(H^+)$.

4. O^+ ions are heated more efficiently than H^+ ions at low altitudes due to pressure cooker effect (Barakat and Barghouthi, 1994). This is also consistent with the zero initial velocity we use for O^+.

5. As polar wind ions heated in the perpendicular direction, part of the energy is converted into the parallel direction, owing to the mirror force, resulting in accelerating the ions in the upward direction. As the ions move upward, the gyroradius at a given energy increases due to the decrease of B, and the gyroradius may become comparable to or exceeds the perpendicular wavelength of the electromagnetic turbulence ($\lambda_\perp$). Above this point, which we call the saturation point, $D_\perp(r, v_\perp)$ decreases very dramatically, and then the heating process decreases.

6. At low altitudes, the wavelength of the electromagnetic turbulence ($\lambda_\perp$) is much greater than the ion gyroradius. Therefore, the simulation results of Barghouthi model are independent of the wavelength of the electromagnetic turbulence ($\lambda_\perp$), i.e. $D_\perp$ is velocity independent, but at high altitudes and above the saturation point, the ions gyroradius may become comparable to or even more than the perpendicular wavelength of the electromagnetic turbulence $\lambda_\perp$, and consequently, the heating of the ions becomes self-limiting. The saturation point for H^+ ions occurs at ($\sim$10.5 R_E) for the perpendicular wavelength of the electromagnetic turbulence $\lambda_\perp = 8$ km. On the other hand, the saturation point for O^+ ions occurs at ($\sim$6.0 R_E) for the same perpendicular wavelength of the electromagnetic turbulence. This is similar to the results of Bouhram et al. (2004) for the cusp: they found the saturation to occur at lower altitude in the cusp (3.5 R_E geocentric distances), consistent with more intense heating in the cusp, so that the ion gyroradius becomes large compared to the wavelength of the electric field turbulence at lower altitudes.

7. Above the saturation point, the ion velocity distribution function displays toroidal features, because the ions tend to move out of the region of large diffusion coefficient ($v_\perp \cong 0$) and accumulate in the region of relatively low diffusion coefficient (i.e. the ions tend to diffuse out of the heating zone in the velocity space). The velocity distribution function of H^+ ions displays toroidal features at ($\sim$12.8 R_E), but for O^+ ions the toroidal features appear at ($\sim$5.97 R_E) for the perpendicular wavelength of the electromagnetic turbulence $\lambda_\perp = 8$ km.

8. The heating process is dramatically reduced above the saturation point, since the ions tend to move out of the region of large diffusion coefficient and accumulate in a region of relatively low diffusion coefficient (i.e. the ions tend to move out of the heating zone into a region of negligible WPI); therefore, the effect of WPI becomes negligible above the saturation point. This is very clear from the saturations of the simulation above saturation point. The model seems to show too much perpendicular heating at the highest altitudes, and future work is needed to decide if the effective wave length should be set to less than 8 km or if the velocity diffusion coefficients should be reduced at high altitude.

9. Since the ion gyroradius will be comparable to or exceeds the wavelength of the electromagnetic turbulence $\lambda_\perp$ at high altitude, also and when $\lambda_\perp$ decreases, the saturation point occurred earlier, and consequently the toroidal features appear at lower altitudes. For H^+ ions, namely for the case $\lambda_\perp = 8$ km, the toroidal features appear at $\sim$12.8 R_E, but for the case $\lambda_\perp = 20$ km at geocentric altitude $\sim$13.7 R_E. For O^+ ions, namely for electromagnetic turbulence wavelength $\lambda_\perp = 20$ km, the toroidal features appear at $\sim$6.66 R_E, but for the case $\lambda_\perp = 8$ km, the toroidal appear at $\sim$5.97 R_E.

10. From the comparison quantitatively and qualitatively between simulation results obtained by using Barghouthi model and observations obtained from different satellites, we found many close agreements between both results for different ions and at different altitudes. Because of this close agreement, we suggest that the characteristic perpendicular wavelength of the electromagnetic turbulence is about 8 km. This claim is consistent with the claim of Barghouthi (2008) in the auroral region.

11. The major discrepancy between observations and the current model relates to the density of O^+ ions, which is severely underestimated. As the drift velocity is approximately right, this means that our number flux is severely underestimated. The number flux is of course strongly affected by the number flux at the lower boundary. We have used zero drift velocity as boundary condition, because this is consistent with the average value

of observations. The observations show low averages because the ions are gravitationally bound and a significant fraction is moving downward, which is true also in the model. We have argued that most of these ions will mirror and eventually move upward. The number flux from the initial source must be as high as is required to match the number fluxes observed at high altitude. It may be better to set our drift velocity to a small positive value that is consistent with the total number fluxes observed at higher altitudes rather than trying to keep close to observed estimates of the drift velocity. Another possibility is that because O^+ ions have a low parallel velocity at low altitude, they drift long distances and the difference between auroral zone/cusp origin and polar cap origin becomes smeared. It is therefore possible that the number fluxes of O^+ at high altitude should be compared to cusp outflow rather than low altitude polar wind outflow. A proper estimate of the effect of convection is needed to determine this. If outflow is slow enough, polar cap O^+ outflow would end up in the lobes rather than geometrically above the polar cap.

12. We have compared our model results with many different observations obtained for different geophysical and solar cycle conditions. The observations reported by Su et al. (1998) and Chugunin (2009) were obtained at solar minimum. The observations reported by Nagai et al. (1984), Nilsson et al. (2008) and Engwall et al. (2009) were obtained at solar maximum. The Akebono results reported, for example, by Abe et al. (1993) were obtained for a full solar cycle. The model agrees fairly well with all these observations. This is not a proof that there is no significant solar cycle dependence of the ion outflow, but it does justify using one set of boundary conditions to obtain a reference model from which observations from both low and high solar activity can be compared.

Finally, in addition to this comparison, Barghouthi model simulations will be compared to other observations, and then extended according to what we learn from these comparisons. The model simulation results will almost certainly lead us to search for new details in the observations. For example, from the above comparisons we claim that the perpendicular wavelength of the electromagnetic turbulence is approximately 8 km; this claim will guide us in searching the data for new information on the characteristics of the electromagnetic turbulence.

Acknowledgements. This research was supported by Swedish Research Links program, Swedish research council, Stockholm, Sweden.

Topical Editor R. Nakamura thanks two anonymous referees for their help in evaluating this paper.

References

Abe, T., Whalen, B. A., Yau, A. W., Horita, R. E., Watanabe, S., and Sagawa, E.: EXOS D (Akebono) Suprathermal mass spectrometer observations of the polar wind, J. Geophys. Res., 98, 11191–11203, 1993.

Abe, T., Watanabe, S., Whalen, B. A., Yau, A. W., and Sagawa, E.: Observations of Polar Wind and Thermal Ion Outflow by Akebono/SMS, J. Geomag. Geoel., 48, 319–325, 1996.

Abe, T., Yau, A. W., Watanabe, S., Yamada, M., and Sagawa, E.: Long-term variation of the polar winds velocity and its implication for the ion acceleration process: Akebono/suprathermal ion mass spectrometer observations, J. Geophys. Res., 109, A09035, doi:10.1029/2003JA010223, 2004.

Axford, W. I.: The polar wind and the terrestrial helium budget, J. Geophys. Res., 73, 6855–6859, 1968.

Barakat, A. R. and Barghouthi, I. A.: The effects of wave-particle interactions on the polar wind O^+, Geophys. Res. Lett., 21 2279–2282, 1994.

Barakat, A. R. and Lemaire, J.: Monte Carlo study of the escape of a minor species, Phys. Rev. A., 42, 3291–3302, 1990.

Barakat, A. R. and Schunk, R. W.: O^+ ions in the polar wind, J. Geophys. Res., 88, 7887–7894, 1983.

Barghouthi, I. A.: Effects of wave particle interactions on H^+ and O^+ outflow at high latitude; A comparative study, J. Geophys. Res., 102, 22062–22075, 1997.

Barghouthi, I. A.: A Monte Carlo study for ion outflows at high altitude and high latitude: Barghouthi model, J. Geophys. Res., 113, A08209, doi:10.1029/2008JA013274, 2008.

Barghouthi, I. A. and Atout, M. A.: Monte Carlo modeling of toroidal ion distributions and ion temperatures at high altitudes equatorward of the cusp: Effect of finite gyroradius, J. Geophys. Res., 111, A03202, doi:10.1029/2005JA011437, 2006.

Barghouthi I. A., Barakat, A. R., and Persoon, A. M.: The effects of altitude-dependent wave particle interactions on the polar wind plasma, Astrophysics and Space Sciences, 259, 117–140, doi:10.1023/A:1001569207346, 1998.

Bouhram, M., Malingre, M., Jasperse, J. R., and Dubouloz, N.: Modeling transverse heating and outflow of ionospheric ions from the dayside cusp/cleft. 1 A parametric study, Ann. Geophys., 21, 1753–1771, doi:10.5194/angeo-21-1753-2003, 2003a.

Bouhram, M., Malingre, M., Jasperse, J. R., Dubouloz, N., and Sauvaud, J.-A.: Modeling transverse heating and outflow of ionospheric ions from the dayside cusp/cleft. 2 Applications, Ann. Geophys., 21, 1773–1791, doi:10.5194/angeo-21-1773-2003, 2003b.

Bouhram, M., Klecker, B., Miyake, W., Rème, H., Sauvaud, J.-A., Malingre, M., Kistler, L., and Blăgău, A.: On the altitude dependence of transversely heated O^+ distributions in the cusp/cleft, Ann. Geophys., 22, 1787–1798, doi:10.5194/angeo-22-1787-2004, 2004.

Chandler, M. O., Waite Jr., J. H., and Moore, T. E.: Observations of polar ion outflows, J. Geophys. Res., 96, 1421–1428, 1991.

Chang, T. and Coppi, B.: Lower hybrid acceleration and ion evolution in the suprauroral region, Geophys. Res. Lett., 8, 1253–1256, 1981.

Chang, T., Crew, G. B., Hershkowitz, N., Jasperse, J. R., Retterer, J. M., and Winningham, J. D.: Transverse acceleration of oxygen ions by electromagnetic ion cyclotron resonance with broadband left-hand polarized waves, Geophys. Res. Lett., 13, 636–

639, 1986.

Chugunin, D. V.: Characteristics of thermal ion outflows in the polar cap according to data of the Interball-2 satellite, Cosmic Research, 47, 449–459, 2009.

Crew, G. B., Chang, T., Retterer, J. M., Peterson, W. K., Gurnett, D. A., and Huff, R. L.: Ion cyclotron resonance heated conics: Theory and observations, J. Geophys. Res., 95, 3959–3985, 1990.

Demars, H. G., Barakat, A. R., and Schunk, R. W.: Effect of centrifugal acceleration on the polar wind, J. Geophys. Res., 101, 24565–24571, 1996.

Drakou, E., Yau, A. W., and Abe, T.: Ion temperature measurements from the Akebono suprathermal mass spectrometer: Application to the polar wind, J. Geophys. Res., 102, 17523–17539, 1997.

Elliott, H. A., Comfort, R. H., Creaven, P. D., Chandler, M. O., and Moore, T. E.: Solar wind influence on the oxygen content of ion outflow in the high altitude polar cap during solar minimum conditions, J. Geophys. Res., 106, 6067–6084, 2001.

Engwall, E., Eriksson, A. I., Cully, C. M., André, M., Puhl-Quinn, P. A., Vaith, H., and Torbert, R.: Survey of cold ionospheric outflows in the magnetotail, Ann. Geophys., 27, 3185–3201, doi:10.5194/angeo-27-3185-2009, 2009.

Green, J. L. and Waite Jr., J. H.: On the origin of polar ion streams, Geophys. Res. Lett., 12, 149–152, 1985.

Gurgiolo, C. and Burch, J. L.: DE-1 observations of the polar wind – A heated and unheated component, Geophys. Res. Lett., 9, 945–948, 1982.

Hoffman, J. H. and Dobson, W. H.: Light ion concentrations and fluxes in the polar region during magnetically quiet times, J. Geophys. Res., 85, 626–632, 1980.

Horwitz, J. L., Ho, C. W., Scarbro, H. D., Wilson, G. R., and Moore, T. E.: Centrifugal acceleration of the *polar* wind, J. Geophys. Res., 99, 15051–15064, 1994.

Huddleston, M. M., Pollock, C. J., Wuest, M. P., Pichett, J. S., Moore, T. E., and Peterson, W. K.: Toroidal ion distributions observed at high altitudes equatorward of the cusp, Geophys. Res. Lett., 27, 469–472, 2000.

Lemaire, J. F., Peterson, W. K., Chang, T., Schunk, R. W., Barakat, A. R., Demars, H. G., and Khazanov, G, V.: History of kinetic polar wind models and early observations, in: Recent Advances in the Polar Wind Theories and Observations, edited by: Tam, S. W., Pierrard, V., and Schunk, R. W., J. Atmos. Solar-Terr. Phys., 69, 1901–1935, 2007.

Moore, T. E. and Delcourt, D. C.: Transport and energization of ionospheric plasma (Abstract), Full Meet. Suppl., Eos Trans. AGU, 73, 471, 1992.

Nagai, T., Waite, J. H., Green, J. L., and Chappell, C. R.: First measurement of supersonic polar wind in the polar magnetosphere. Geophys. Res. Lett., 11, 669–672, 1984.

Nilsson, H., Waara, M., Arvelius, S., Marghitu, O., Bouhram, M., Hobara, Y., Yamauchi, M., Lundin, R., Rème, H., Sauvaud, J.-A., Dandouras, I., Balogh, A., Kistler, L. M., Klecker, B., Carlson, C. W., Bavassano-Cattaneo, M. B., and Korth, A.: Characteristics of high altitude oxygen ion energization and outflow as observed by Cluster: a statistical study, Ann. Geophys., 24, 1099–1112, doi:10.5194/angeo-24-1099-2006, 2006.

Nilsson, H., Waara, M., Marghitu, O., Yamauchi, M., Lundin, R., Rème, H., Sauvaud, J.-A., Dandouras, I., Lucek, E., Kistler, L. M., Klecker, B., Carlson, C. W., Bavassano-Cattaneo, M. B., and Korth, A.: An assessment of the role of the centrifugal acceleration mechanism in high altitude polar cap oxygen ion outflow, Ann. Geophys., 26, 145–157, doi:10.5194/angeo-26-145-2008, 2008.

Nilsson, H., Engwall, E., Eriksson, A., Puhl-Quinn, P. A., and Arvelius, S.: Centrifugal acceleration in the magnetotail lobes, Ann. Geophys., 28, 569–576, doi:10.5194/angeo-28-569-2010, 2010.

Northrop, T. G.: The adiabatic motion of charged particles, Interscience Publishers, N.Y., 1963.

Persoon, A. M., Gurnett, D. A., and Shawhan, S. D.: Polar cap electron densities from DE-1 plasma wave observations, J. Geophys. Res., 88, 10123–10136, 1983.

Retterer, J. M., Chang, T., and Jasperse, J. R.: Ion acceleration in the suprauroral region: A Monte Carlo Model, Geophys. Res. Lett., 10, 583–586, 1983.

Retterer, J. M., Chang, T., Crew, G. B., Jasperse, J. R., and Winningham, J. D.: Monte Carlo modeling of oxygen ion conic acceleration by cyclotron resonance, Phys. Rev. Lett., 59, 148–151, 1987a.

Retterer, J. M., Chang, T., Crew, G. B., Jasperse, J. R., and Winningham, J. D.: Monte Carlo modeling of oxygen ion conic acceleration by cyclotron resonance with broadband electromagnetic turbulence, in: Physics of space plasma, SPI Conf. Proc. and Reprint Ser., No. 6, edited by: Chang, T., Belcher, J., Jasperse, J. R., and Crew, G., pp. 97–111, Scientific, Cambridge, Mass., 1987b.

Retterer, J. M., Chang, T., and Jasperse, J. R.: Transversely accelerated ions in topside ionosphere, J. Geophys. Res., 99, 13189–13201, 1994.

Slapak, R., Nilsson, H., Waara, M., André, M., Stenberg, G., and Barghouthi, I. A.: O^+ heating associated with strong wave activity in the high altitude cusp and mantle, Ann. Geophys., 29, 931–944, doi:10.5194/angeo-29-931-2011, 2011.

Su, Y. J., Horwitz, J. L., and Moore, T. L.: Polar wind survey with the Thermal Ion Dynamics Experiment/Plasma Source Instrument suite aboard POLAR, J. Geophys. Res., 103, 29305–29337, 1998.

Tam, S. W. Y., Chang, T., and Pierrard, V.: Kinetic modeling of the polar wind, J. Atmos. Solar Terr. Phys., 69, 1984–2027, 2007.

Waara, M., Nilsson, H., Stenberg, G., André, M., Gunell, H., and Rème, H.: Oxygen ion energization observed at high altitudes, Ann. Geophys., 28, 907–916, doi:10.5194/angeo-28-907-2010, 2010.

Waite Jr., J. H., Nagai, T., Johnson, J. F. E., Chappell, C. R., Burch, J. L., Killeen, T. L., Hays, P. B., Carignan, G. R., Peterson, W. K., and Shelley, E. G.: Escape of suprathermal O^+ ions in the polar cap, J. Geophys. Res., 90, 1619–1630, 1985.

Winningham, J. D. and Burch, J.: Observations of large-scale ion conic generation with DE-1, Phys. Space Plasmas, 5, 137–158, 1984.

Yau, A. W. and Andre, M.: Sources of ion outflow in the high latitude ionosphere, Space Sci. Rev., 80, 1–25, 1997.

Yau, A. W., Abe, T., and Peterson, W. K.: The polar wind: Recent observations, J. Atmos. Solar Terr. Phys., 69, 1936–1983, 2007.